

# Hinge non-Hermitian skin effect in the single-particle properties of a strongly correlated $f$ -electron system

Robert Peters<sup>1,\*</sup> and Tsuneya Yoshida<sup>1,2</sup>

<sup>1</sup>*Department of Physics, Kyoto University, Kyoto 606-8502, Kyoto, Japan*

<sup>2</sup>*Institute for Theoretical Physics, ETH Zurich, 8093 Zurich, Switzerland*

(Dated: June 13, 2024)

Non-Hermitian systems exhibit novel phenomena without Hermitian counterparts, such as exceptional points and the non-Hermitian skin effect. These non-Hermitian topological phenomena are observable in single-particle excitations of correlated systems in equilibrium, which are described by Green's functions. In this paper, we demonstrate the appearance of the hinge non-Hermitian skin effect in the effective Hamiltonian that describes the single-particle properties of an  $f$ -electron system. Skin effects result in a strong sensitivity to boundary conditions, and a large number of eigenstates localize at one boundary when open boundary conditions are applied. Our system exhibits such sensitivity and hosts skin modes localized around hinges. This hinge skin effect is induced by a non-Hermitian topology of the surface Brillouin zone. The hinge skin modes are observed for one-dimensional subsystems located between one pair of exceptional points in the surface Brillouin zone. This paper highlights that correlated materials are an exciting platform for analyzing non-Hermitian phenomena.

## I. INTRODUCTION

Quantum systems are often inherently open and subject to dissipative processes. Non-Hermitian operators naturally describe such open quantum systems, where energy, i.e., the eigenvalues of the Hamiltonian, are not necessarily real-valued. These complex-valued band structures offer novel topological features that do not have Hermitian equivalents.<sup>1-9</sup> These features include the exceptional point (EP)<sup>10-20</sup> and the non-Hermitian skin effect (NHSE).<sup>21-40</sup> The EP represents a band touching with a degeneracy of the eigenstates, which makes the Hamiltonian non-diagonalizable. On the other hand, the NHSE's extreme sensitivity of eigenvalues and eigenstates originate from non-trivial point-gap topology in the bulk. The localized boundary modes under open boundary conditions are known as skin modes. Non-Hermiticity is not limited to open quantum systems.<sup>41-45</sup> It also appears in various other systems, such as photonic crystals,<sup>13,46-56</sup> electric circuits,<sup>57-61</sup> and correlated systems.<sup>17,62-71</sup>

Recent studies have revealed the non-Hermitian aspects of correlated materials. The reason for these non-Hermitian aspects is that observable quantities are often based on single-particle or two-particle operators, which can be expressed by single-particle or two-particle Green's functions, respectively. Because single-particle states or two-particle states obtain a finite lifetime due to scattering, the effective Hamiltonians describing single-particle and two-particle Green's functions are naturally non-Hermitian in correlated materials. Therefore, non-Hermitian effects have an impact on the single-particle

and two-particle properties that are described by the corresponding Green's functions. The effective Hamiltonian describing the single-particle properties of correlated materials includes the self-energy, generally, a complex-valued non-Hermitian matrix.<sup>64,72-74</sup> The complex-valued eigenvalues of this effective Hamiltonian are related to the density of states, and the eigenstates affect single-particle observables. For example, correlation effects in heavy-fermion systems lead to the emergence of EPs and a change of the band structure near the Kondo temperature.<sup>64,66,69</sup> Furthermore, it has been demonstrated that the NHSE can occur in the single-particle Green's function.<sup>62,63,68</sup>

In Ref. 75, it has been demonstrated that due to the enhancement of correlation effects at the surface, localized EPs appear on the surface of a topological Kondo insulator for a specific temperature range. Because the imaginary part of the self-energy in the bulk of the material is smaller, EPs only exist on the surface but not in the bulk. In this paper, we utilize this observation and demonstrate that these surface EPs can lead to the emergence of a hinge NHSE in the same temperature range. Hinge skin modes are, thereby, eigenstates that are localized along the edge of a surface, i.e., these skin modes are localized along a 1D manifold in a 3D system.<sup>25,76-80</sup>

The argument for the occurrence of a hinge NHSE is as follows (also see Fig. 1 for a schematic depiction): (1) EPs appear in the effective single-particle Hamiltonian on the surface of the material. (2) These EPs induce a non-trivial point-gap topology for a one-dimensional subsystem of the surface Brillouin zone (BZ), i.e., paths in the

surface BZ passing in between one pair of EPs. (3) The above subsystem on the surface is topologically equivalent to the Hatano-Nelson model<sup>21,81</sup> and thus exhibits an NHSE. As this NHSE only occurs in a subsystem of the surface BZ, we can conclude the existence of a hinge NHSE in the effective Hamiltonian describing the single-particle properties of a correlated material.

The remainder of this paper is organized as follows. In Sec. II, we introduce the model and methods used. In Sec. III A, we prove the existence of EPs on the surface of this system. This is followed by the demonstration of the NHSE on the surface for a range of momenta in Sec. III B. Finally, in Sec. IV, we summarize and conclude this paper.

## II. MODEL AND METHOD

### A. Model

In this section, we explain the details of the used model. We start with the cubic topological Kondo insulator model, which was analyzed in Refs. 75 and 82. In previous works, it was shown that this model is a three-dimensional strong topological insulator with three surface Dirac cones on each surface. Furthermore, it was demonstrated that EPs in the single-particle Green's function appear on the surface for a specific range of temperatures.<sup>75</sup> For open boundary conditions (OBC) in the  $z$  direction and periodic boundary conditions (PBC) in the  $x$  and  $y$  directions, eight EPs surround the Dirac cone on the  $z$  surface; the winding number takes  $W = +1$  for four of these EPs and  $W = -1$  for the others [see Fig. 1(a)]. A branch cut of eigenvalues connects an EP with winding number  $W = +1$  and another EP with  $W = -1$ , which form a pair. Because of the cubic symmetry of this model, most straight paths in the BZ pass in between two pairs of EPs or none. We modify this model here because we expect the occurrence of a hinge NHSE if a path through the BZ (a one-dimensional subsystem of the surface BZ) passes in between exactly one pair of EPs, i.e., intersects one branch cut between two EPs. In the modified model, the nearest-neighbor hopping depends on the direction, i.e.,  $t_x$ ,  $t_y$ , and  $t_z$  are different. For the parameters chosen here, two pairs of EPs vanish [see Fig. 1(b)]. We expect that such a modification of the model can be achieved by strain.

Next, we include a small magnetic field  $B$  in the  $z$  direction, which creates a gap in the Dirac cone on the  $z$  surface. We include this magnetic field to demonstrate that the appearance of the hinge NHSE is not related to the time-reversal symmetry or Hermitian topology.

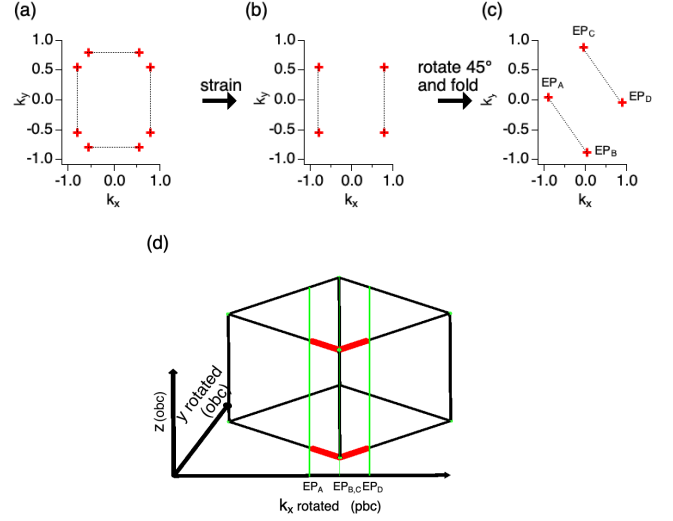


Figure 1. Schematic explanation of the model and the appearance of the hinge NHSE. Panel (a) shows the positions of EPs of the original cubic interacting model at finite temperatures.<sup>75</sup> Two EPs with winding numbers  $+1$  and  $-1$  form a pair. We visualize these pairs by connecting the corresponding EPs by a black line. Panel (b) shows the model where the cubic symmetry is broken by strain, reducing the number of surface EPs. Panel (c) shows the expected positions of EPs in the rotated, strained, and interacting model at finite temperatures. Panel (d) shows the hinge NHSE. We use OBC in the  $z$  and  $y$  directions and PBC in the  $x$  direction. Eigenstates (colored red) are expected to localize in the rotated system on the  $z$  surfaces for a specific range of momenta in the surface BZ. The green lines correspond to the  $k_x$  momenta at which EPs appear in panel (c).

The model Hamiltonian of this system reads

$$H = H_0 + H_{\text{int}}, \quad (1)$$

$$H_0 = \sum_{\vec{k}} \sum_{\sigma=\{\uparrow,\downarrow\}} \sum_{o=\{c,f\}} \epsilon_{\vec{k}}^o c_{\vec{k},\sigma,o}^\dagger c_{\vec{k},\sigma,o} + V \sum_{\vec{k},\tau_1,\tau_2} c_{\vec{k},\tau_1,c}^\dagger c_{\vec{k},\tau_2,f} \sin k_x \sigma_{\tau_1\tau_2}^x + V \sum_{\vec{k},\tau_1,\tau_2} c_{\vec{k},\tau_1,c}^\dagger c_{\vec{k},\tau_2,f} \sin k_y \sigma_{\tau_1\tau_2}^y + V \sum_{\vec{k},\tau_1,\tau_2} c_{\vec{k},\tau_1,c}^\dagger c_{\vec{k},\tau_2,f} \sin k_z \sigma_{\tau_1\tau_2}^z + B \sum_{\vec{k},\tau_1,\tau_2,o} c_{\vec{k},\tau_1,o}^\dagger c_{\vec{k},\tau_2,o} \sigma_{\tau_1\tau_2}^z + \sum_{i,\sigma,o} E^o n_{i,\sigma,o}, \quad (2)$$

$$+ \sum_{i,\sigma,o} E^o n_{i,\sigma,o}, \quad (3)$$

where the energy dispersion  $\epsilon_k^o$  is given as

$$\begin{aligned} \epsilon_k^c &= -2t_x \cos(k_x) - 2t_y \cos(k_y) - 2t_z \cos(k_z) \\ &\quad + 4t' \cdot \cos(k_x) \cos(k_y) \\ &\quad + 4t' \cdot \cos(k_y) \cos(k_z) \\ &\quad + 4t' \cdot \cos(k_x) \cos(k_z) \\ &\quad + 8t'' \cdot \cos(k_x) \cos(k_y) \cos(k_z), \\ \epsilon_k^f &= -0.1\epsilon_k^c. \end{aligned} \quad (4)$$

The operator  $c_{\vec{k},\sigma,o}^\dagger$  ( $c_{\vec{k},\sigma,o}$ ) creates (annihilates) an electron with momentum  $\vec{k}$ , spin direction  $\sigma = \{\uparrow, \downarrow\}$  in orbital  $o \in \{c, f\}$ .  $t_a$ ,  $t'$ , and  $t''$  are nearest-neighbor, next-nearest-neighbor, and next-next-nearest-neighbor hopping constants.  $V$  corresponds to a nonlocal hybridization between the  $f$  and  $c$  electrons,  $B$  is a magnetic field in the  $z$  direction, and  $E^o$  are energy shifts depending on the orbital ( $f$  or  $c$  electrons). The local two-particle interaction for the  $f$  electrons reads

$$H_{\text{int}} = U \sum_i n_{i,\uparrow,f} n_{i,\downarrow,f}. \quad (5)$$

We note that this Hamiltonian is Hermitian. In this paper, we use the following parameters:  $t_x/|t_z| = -1.24$ ,  $t_y/|t_z| = -0.76$ ,  $t_z = -1$ ,  $t'/|t_z| = t''/|t_z| = 0.375$ ,  $V/|t_z| = 0.8$ ,  $B/|t_z| = 0.002$ ,  $E^c/|t_z| = -1$ ,  $U/|t_z| = 16$ , and  $E^f/|t_z| = -8$ . The temperature is fixed to  $T/|t_z| = 0.108$ . We use the strength of the hopping in the  $z$  direction,  $|t_z|$ , as the energy unit throughout this paper. We note that the Dirac cones at  $(k_x, k_y) = (0, 0)$ ,  $(\pi, 0)$ , and  $(0, \pi)$  are gapped by the small magnetic field. The expected positions of the EPs on the  $z$  surface (OBC in the  $z$  direction, PBC in the  $x$  and  $y$  directions) of the original model<sup>75</sup> and the modified model are shown in Fig. 1(a) and Fig. 1(b). As explained above, we expect that the number of surface EPs will be reduced from eight to four in the interacting model at finite temperature. Furthermore, EPs connected by a branch cut, on which the real parts of two eigenvalues are identical, are linked by black lines in the schematic pictures of Fig. 1.

Finally, we rotate this model in real space by  $45^\circ$ . This rotation leads to a change in the positions of the EPs on the surface BZ, as shown in Fig. 1(c). To obtain a periodic  $45^\circ$ -rotated system, we double the unit cell, resulting in a folding of the band structure. The noninteracting band structure of this model, using the  $45^\circ$ -rotated geometry, is shown in Fig. 2. After this rotation, we expect that there are straight paths along the  $k_x$  or the  $k_y$  direction through the BZ that pass in between exactly one pair of EPs. These paths fulfill the necessary conditions for the

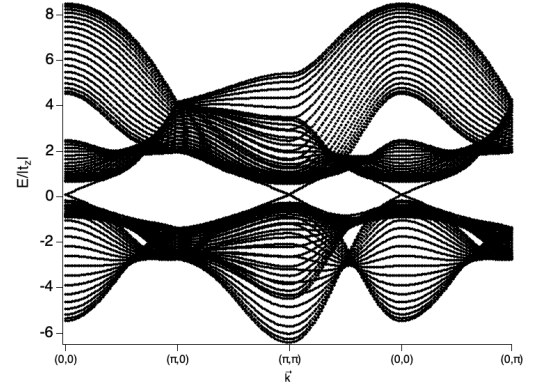


Figure 2. Noninteracting band structure of the strained rotated model. Dirac cones appear for OBC in the  $z$  direction at  $\vec{k} = (0, 0)$  and  $(\pi, \pi)$ .

appearance of the NHSE, which is the main topic of this paper. In the results section, we will numerically demonstrate the emergence of these EPs and the appearance of the hinge NHSE.

## B. Method

To solve this model, we use real-space dynamical mean-field theory (DMFT). DMFT maps each atom of a lattice on an effective quantum impurity model.<sup>83–85</sup> This mapping neglects nonlocal correlations. Because we use OBC in the  $z$  direction throughout this paper, correlation effects and, thus, self-energies depend on the distance of the atom from the surface in the  $z$  direction. We thus map each layer on its own quantum impurity model.<sup>86</sup> These impurity models are solved by the numerical renormalization group,<sup>87,88</sup> from which we obtain the layer-dependent self-energies at finite temperatures. Using these self-energies, we can determine new effective impurity models. This DMFT cycle is iterated until self-consistency is reached.

Having obtained self-consistent self-energies, we determine the effective Hamiltonian describing the single-particle properties by the single-particle Green's function as

$$G(\omega) = (\omega + i\eta - H_{\text{eff}})^{-1}, \quad (6)$$

$$H_{\text{eff}} = H_0 + \Sigma(\omega), \quad (7)$$

where  $\omega$  is the frequency,  $H_0$  is the noninteracting Hamiltonian,  $\eta$  is an infinitesimal small, positive adiabatic factor, and  $\Sigma(\omega)$  is the self-energy. We note that the self-energy

depends on the layer, orbital ( $f$  or  $c$ ), and the spin direction. Thus,  $H_{\text{eff}}$  is a matrix. Furthermore, this matrix is a non-Hermitian matrix due to the imaginary part of the self-energy. Because the self-energy is frequency-dependent, the effective Hamiltonian also depends on the frequency. In this paper, we focus on the Fermi energy,  $\omega = 0$ , and use  $\Sigma(\omega = 0)$ . The single-particle properties of this system are completely determined by the eigenvalues and eigenstates of this effective Hamiltonian. The single-particle properties at the Fermi energy are thereby mostly given by the eigenvalues with  $\text{Re}(E_i) \approx 0$  because then  $\text{Re}(\omega - E_i) \approx 0$ . Thus, we will focus on the eigenvalues of the effective Hamiltonian with a small real part.

The matrix of the effective Hamiltonian depends on the boundary conditions. We will generally use OBC with 20 layers in the  $z$  direction. To demonstrate the hinge NHSE, we will use two different kinds of boundary conditions in the  $x$  and  $y$  directions of the rotated system. First, we will show results for PBC in the  $x$  and  $y$  directions. Second, we will show results for PBC in the  $x$  direction and OBC with 40 atoms in the  $y$  direction.

### III. RESULTS

#### A. Energy spectrum of the rotated model

In this section, we numerically confirm that EPs emerge as illustrated in Fig. 1(c). We analyze the energy spectrum and eigenstates of the effective Hamiltonian, Eq. (7), describing the single-particle Green's function in the interacting model at temperature  $T/|t_z| = 0.108$ .

Figure 3 shows the real part of the eigenvalues of the effective Hamiltonian,  $H_{\text{eff}}(\omega = 0)$ , for OBC in the  $z$  direction and PBC in the  $x$  and  $y$  directions. From Fig. 3(a), it becomes clear that the self-energy arising from correlation effects has a large impact, especially around the Fermi energy. Low-energy eigenstates exist around  $(k_x, k_y) = (0, 0)$  and  $(\pi, \pi)$ , the original position of the Dirac cones in the rotated model, but their shape has changed due to the self-energy. In Figs. 3(b) and 3(c), we show the real part of the eigenvalues over the whole BZ and a magnification around  $(k_x, k_y) = (0, 0)$ , respectively. We see a band surrounding  $(k_x, k_y) = (0, 0)$ . In the magnification of this band, shown in Fig. 3(c), we see that this band is open and not completely surrounding the  $\Gamma$  point. Additionally, we have marked the momentum values with degenerate real parts of the eigenvalue as yellow points. This line of eigenvalues with degenerate real parts suddenly ends. The end points are marked as green dots. Such an abrupt ending of a band in the BZ, which is impossible in a noninteracting model, is the first

evidence of EPs (green dots). As two EPs are connected by a band of eigenvalues with degenerate real parts in the BZ, always two EPs form a pair. In Fig. 1, we have drawn lines between EPs forming pairs.

To prove the existence of EPs in the effective Hamiltonian, we calculate a quantity describing the defectiveness of a matrix,

$$D = \max_{i \neq j} \frac{1}{1 - |\langle \Psi_{R,i} | \Psi_{R,j} \rangle|} \quad (8)$$

and show it in Fig. 4.  $|\Psi_{R,i}\rangle$  is the  $i$ -th right-eigenstate of the effective Hamiltonian. The right-eigenstates are normalized as  $\langle \Psi_{R,i} | \Psi_{R,i} \rangle = 1$ . This property diverges if two eigenstates of the effective Hamiltonian are identical, although these eigenstates belong to different eigenvalues ( $i \neq j$ ). The fact that two different eigenstates are identical is evidence of an EP. In Fig. 4(a), we see that this property diverges at four momenta in the BZ. We can conclude that there are four EPs in the BZ. We show the positions of these EPs as green dots in Fig. 3. This result confirms that our expectation in Fig. 1(c) was correct. We furthermore show the absolute value of the eigenstates at the EPs over the layer index  $z$  in Fig. 4(b). We see that these eigenstates are localized on the top and bottom surfaces in the  $z$  direction.

We note that these EPs are stable while the Dirac cone is gapped due to the magnetic field and further altered by the self-energy. Small changes in the Hamiltonian, even breaking the time-reversal symmetry, do not annihilate these EPs in the effective Hamiltonian.

#### B. Hinge skin effect induced by surface EPs

We demonstrate the occurrence of the NHSE for specific momenta in the system when the path through the surface BZ passes in between one pair of EPs.

In Fig. 5, we show the eigenvalues of the effective Hamiltonian using PBC in the  $x$  direction and compare the results obtained using OBC and PBC in the  $y$  direction. In Fig. 5(a) and 5(b), we fix the momentum in the  $x$  direction to  $k_x = -0.5$ , specifying a path that intersects a branch cut between a pair of EPs when changing the  $y$  direction. In Fig. 5(c) and 5(d), we use  $k_x = -1$ , specifying a path that does not intersect a branch cut between two EPs. In Fig. 5(a) and 5(c), we show the imaginary part of the eigenvalues over the real part. The black points denote the PBC spectrum, and the green points denote the OBC spectrum with 40 sites in the  $y$  direction. In Fig. 5(b) and 5(d), we furthermore show the winding of the spectrum around a reference energy  $E_0 (\in \mathbb{C})$  defined

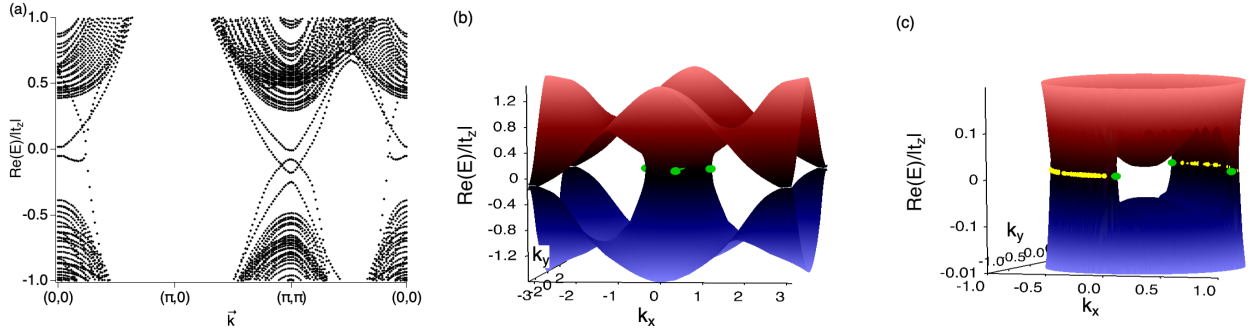


Figure 3. Real part of the eigenvalues of the effective Hamiltonian at the Fermi energy. Panel (a) shows the real part of the eigenvalues close to the Fermi energy along a path in the BZ. Panel (b) shows the real part of the eigenvalues over the full BZ. Panel (c) shows a magnification of (b) around the  $(k_x, k_y) = (0, 0)$  close to the Fermi energy. The color in panels (b) and (c) corresponds to the real part of the energy and is just used to improve visualization. Yellow dots denote a line of momenta connected to the EPs, where the real part of the eigenvalues is degenerate. The green dots correspond to the position of the EPs, where the line of degeneracies ends. All results are for OBC in the  $z$  direction and PBC in the  $x$  and  $y$  directions.

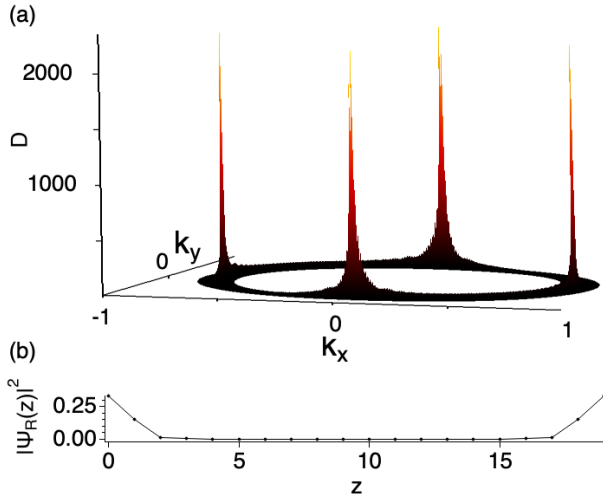


Figure 4. Evidence of EPs in the surface BZ. Panel (a) shows  $D$ , defined in Eq. (8), which diverges at an EP. Panel (b) shows the square of the absolute value of the eigenstates at each EP [divergence in panel (a)] over the layer index  $z$ . The  $z$  dependence, which is identical at all four EPs, demonstrates that the eigenstates are localized at the surfaces in the  $z$  direction.

as

$$\omega = \arg[\det(H_{\text{eff}}(k_y) - E_0 I)], \quad (9)$$

which is related to the winding number as

$$W = \oint \frac{dk_y}{2\pi} \cdot \partial_{k_y} \arg[\det[H_{\text{eff}}(k_y) - E_0 I]]. \quad (10)$$

For  $k_x = -0.5$  [see Fig. 5(a)], we see that there are PBC bands connecting the bulk bands for  $\text{Re}(E)/|t_z| < -0.4$  with the bulk bands  $\text{Re}(E)/|t_z| > 0.4$ . These bands clearly form a loop structure, i.e., a point gap opens. We have confirmed that the eigenstates forming this loop structure for  $|\text{Re}(E)/|t_z|| < 0.4$  are located on the  $z$  surface and that the bottom and top layers contribute to these eigenstates. The layer dependence of the eigenstates in this region is thereby similar to the eigenstates shown in Fig. 4(b). To confirm the topological point gap, we calculate the winding in Fig. 5(b) for a reference energy ( $E_0/|t_z| = -1.6i$ ) located inside this point gap. We see that the winding number becomes  $-2$  for this reference energy. This winding number indicates a winding of eigenvalues on the top and bottom  $z$  surfaces. A winding number of  $-2$  is consistent with the fact that these eigenstates are located on the bottom and top surfaces and that both surfaces contribute. Having confirmed the existence of a nontrivial point-gap topology in the energy spectrum, we expect the emergence of the NHSE.<sup>38</sup> Analyzing the OBC spectrum for  $k_x = -0.5$ , we see that this loop structure collapses to a single line in the energy spectrum. This sensitivity of the energy spectrum on the boundary conditions is one of the characteristics of the NHSE.

Before analyzing the OBC eigenstates for  $k_x = -0.5$ , we show the data for  $k_x = -1$ , which corresponds to a path that does not pass in between a pair of EPs. In Fig. 5(c), we see that for  $k_x = -1$  bulk bands above  $\text{Re}(E)/|t_z| > 0.5$  are not connected to bulk bands  $\text{Re}(E)/|t_z| < -0.5$ . Accordingly, the winding around the reference energy ( $E_0/|t_z| = -1.6i$ ) becomes zero. Thus, we expect the absence of the NHSE. However, for OBC,

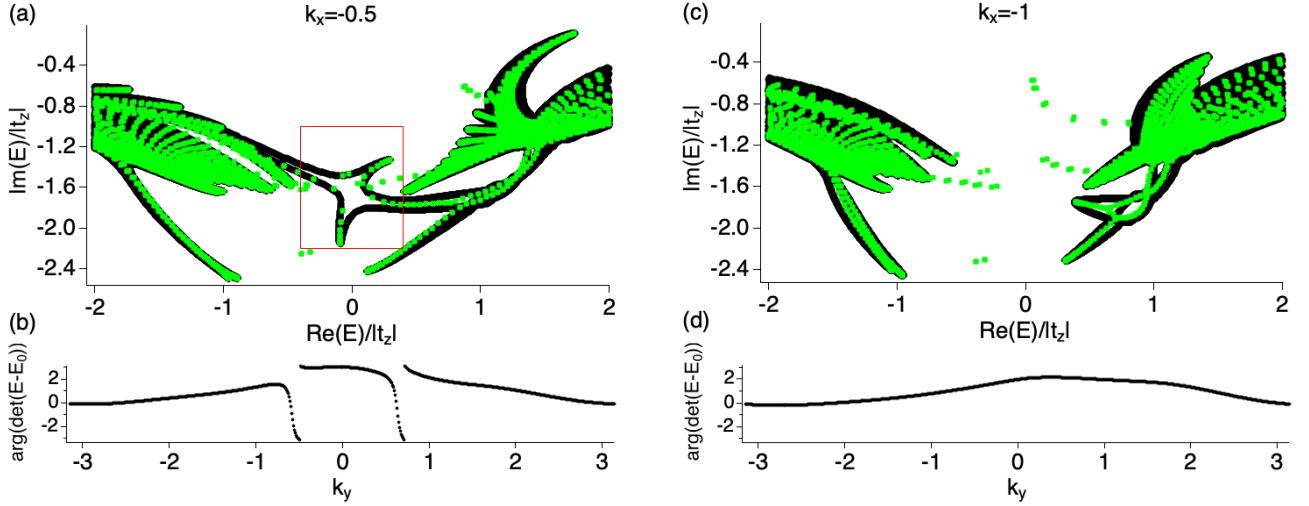


Figure 5. Comparison of PBC and OBC spectra in the  $y$  direction and the corresponding winding around a reference energy  $E_0/|t_z| = 0 - 1.6i$ . We use PBC in the  $x$  direction. Panel (a) compares the PBC spectrum (black) with the OBC spectrum (green) for  $k_x = -0.5$ , resulting in a path through the BZ that intersects one pair of EPs. Clearly visible is a point gap around  $\text{Re}(E) \approx 0$ . We show in Fig. 7 the wavefunctions for all eigenstates inside the red rectangle. Panel (b) shows the winding for the reference energy  $E_0$ . Panel (c) shows the same quantities as (a) but for  $k_x = -1$ . In the PBC spectrum, there is no point gap. Panel (d) shows the absence of any winding for  $k_x = -1$  using the same reference energy as in panel (b).

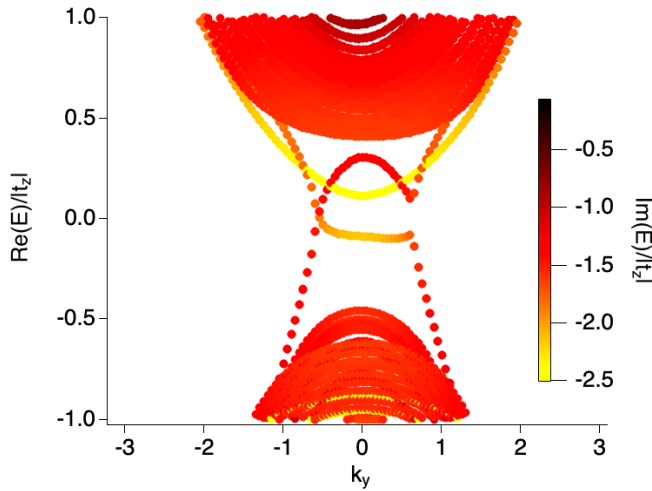


Figure 6. Real parts of the eigenvalues over  $k_y$  (PBC) with  $k_x = -0.5$  resulting in a point gap at  $\text{Re}(E) \approx 0$ . The color corresponds to the imaginary part of the eigenvalues.

there are several states for  $-0.4 < \text{Re}(E)/|t_z| < 0.4$ . These eigenstates are unrelated to the NHSE but originate in the Hermitian noninteracting Hamiltonian, as we demonstrate in Appendix A.

For a better understanding of the nontrivial point gap topology, we show  $\text{Re}(E)$  over  $k_y$  for  $k_x = -0.5$  (PBC) in Fig. 6 again. The color corresponds to the imaginary part of each eigenvalue. We clearly see a crossing of two bands at  $\text{Re}(E) \approx 0$  and  $k_y \approx -0.8$ . This crossing, i.e., a degeneracy of the real part, corresponds to the above-mentioned branch cut connecting two EPs, visualized as yellow dots in Fig. 3(c). Such a crossing exists only for paths that pass in between a pair of EPs. Thus, there exists only one crossing because this crossing is generated by the EPs. From the color in Fig. 6, we see that the imaginary parts of these two crossing bands are different. Thus, these two intersecting bands form the nontrivial point-gap topology in Fig. 5(a).

Finally, we prove the NHSE on the  $z$  surface for  $k_y = -0.5$  by showing the right and left eigenstates for  $-0.4 < \text{Re}(E)/|t_z| < 0.4$  over the position in the  $y$  direction (OBC) in Fig. 7. The plotted eigenstates are restricted to those inside the red rectangle in Fig. 5(a). Figure 7(a) [7(b)] shows the right [left] eigenstates. A large number of right eigenstates (red color) have an increased absolute value,  $|\Psi_R(y)|^2$ , on the right side when compared to the left side. The absolute value of these right eigenvectors has a positive slope over the  $y$  position. The left eigenvectors for the same eigenvalues [colored red in Fig. 7(b)] have a negative slope. We can thus conclude that a large number of right eigenstates are mainly local-

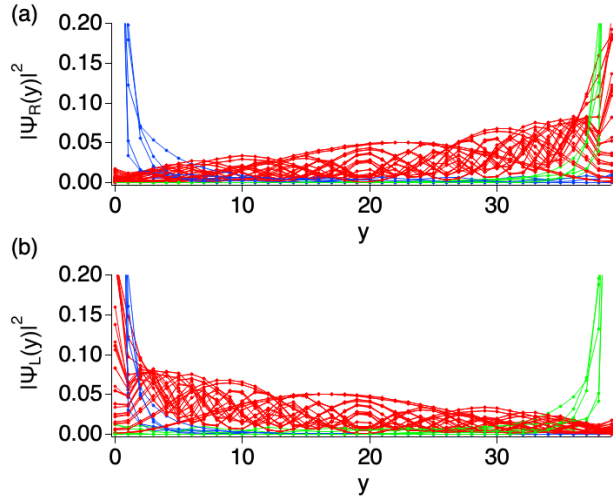


Figure 7. The amplitude of the right and left eigenstates for  $k_y = -0.5$  over the position in the  $y$  direction. We show the right eigenstates,  $|\Psi_R(y)|^2$ , in panel (a) and the left eigenstates,  $|\Psi_L(y)|^2$ , in panel (b). The red eigenstates correspond to the skin modes, where the magnitude of the right (left) eigenstates increases towards the right (left) side. Green and blue eigenstates correspond to localized states remaining from the Dirac cones of the Hermitian noninteracting model. The wave functions are normalized as  $\sum_y |\Psi_{R/L}(y)|^2 = 1$ .

ized on the right side, and the left eigenstates are mainly localized on the left side of the system with open boundaries in the  $y$  direction. This is the expected behavior of the NHSE, in which a large number of left and right eigenstates localize on the opposite edges of the system. We stress that these skin modes localize around a hinge of the three-dimensional system; the localization occurs on the  $z$  surface for a specific range of  $k_x$  values.

Besides these skin modes, there are other eigenstates that localize at the boundaries in the  $y$  direction. These eigenstates maintain their position of localization when changing between right and left eigenstates. In Fig. 7, both right and left eigenstates denoted by green (blue) lines are localized around  $y = 40$  ( $y = 0$ ). These eigenstates arise from the original Hermitian Hamiltonian and are unrelated to non-Hermiticity, as shown in Appendix A. These states can be seen in Fig. 5 as green dots appearing seemingly unrelated to the PBC band structure (black).

## IV. CONCLUSIONS

We have demonstrated the appearance of the hinge NHSE in the effective Hamiltonian, which describes the single-particle Green's function. The used model Hamiltonian is derived from a three-dimensional strong topological Kondo insulator under magnetic field and strains. By showing the energy spectrum along a path passing in between one pair of EPs, we have demonstrated the existence of a nontrivial point-gap topology necessary for the emergence of the NHSE. We furthermore have shown that a large number of right eigenstates localize at the right boundary for OBC in the  $y$  direction, while the corresponding left eigenstates localize at the left boundary. All these skin modes are localized on the boundaries of the top and bottom  $z$  surfaces. Thus, we have demonstrated the emergence of the hinge NHSE in the effective Hamiltonian, describing the single-particle properties of this strongly correlated system.

## ACKNOWLEDGMENTS

R.P. is supported by JSPS KAKENHI No. JP23K03300. T.Y. is supported by JSPS KAKENHI Grant Nos. JP21K13850 and JP23KK0247, JSPS Bilateral Program No. JPJSBP120249925. T.Y. is grateful for the support from the ETH Pauli Center for Theoretical Studies and the Grant from the Yamada Science Foundation. Parts of the numerical simulations in this work have been done using the facilities of the Supercomputer Center at the Institute for Solid State Physics, the University of Tokyo.

## Appendix A: Hermitian boundary states

In this appendix, we analyze the energy spectrum and wave functions in the Hermitian case at  $T = 0$ . At  $T = 0$ , the imaginary part of the self-energy at the Fermi energy vanishes. Thus, the matrix describing the single-particle properties at the Fermi energy becomes Hermitian.

In Fig. 8(a), we show the energy spectrum of the rotated model for OBC in the  $z$  direction and PBC in the  $x$  direction. We compare OBC and PBC in the  $y$  direction. As expected, the imaginary part of the eigenvalues vanishes for the Hermitian matrix. Furthermore, we see that the PBC spectrum includes a gap at the Fermi energy,  $Re(E) = 0$ . When changing to OBC in the  $y$  direction, we see eigenvalues inside this gap. The wave functions of these eigenstates are shown in Fig. 8(b), demonstrat-

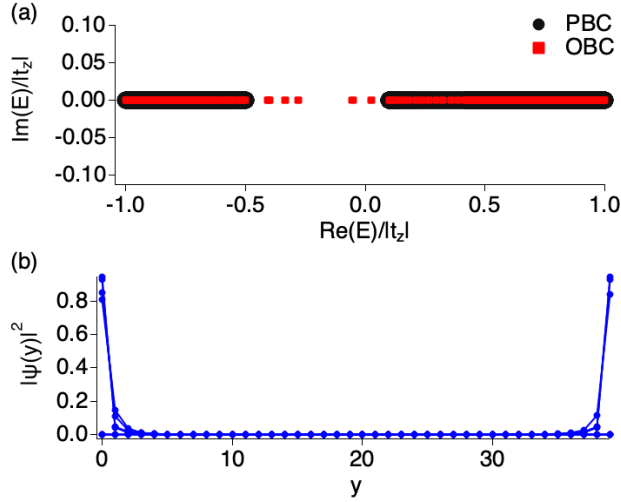


Figure 8. The energy spectrum for OBC and PBC at  $T = 0$ , for the Hermitian effective Hamiltonian. Panel (a) shows the energy spectrum for OBC and PBC. Clearly visible is a gap in the PBC spectrum and in-gap states in the OBC spectrum. Panel (b) shows the wave functions of these in-gap states for OBC in the  $y$  direction. The wave function is normalized as  $\sum_y |\Psi(y)|^2 = 1$ .

ing that these eigenstates are localized at the boundaries in the  $y$  direction. We believe these eigenstates have the same origin as the localized eigenstates in Figs. 7 that do not originate from the NHSE.

\* Correspondence email address: peters.robert.7n@kyoto-u.ac.jp

<sup>1</sup> Zongping Gong, Yuto Ashida, Kohei Kawabata, Kazuaki Takasan, Sho Higashikawa, and Masahito Ueda, “Topological phases of non-hermitian systems,” *Phys. Rev. X* **8**, 031079 (2018).

<sup>2</sup> Ramy El-Ganainy, Konstantinos G. Makris, Mercedeh Khajavikhan, Ziad H. Musslimani, Stefan Rotter, and Demetrios N. Christodoulides, “Non-hermitian physics and  $pt$  symmetry,” *Nature Physics* **14**, 11–19 (2018).

<sup>3</sup> Kohei Kawabata, Ken Shiozaki, Masahito Ueda, and Masatoshi Sato, “Symmetry and topology in non-hermitian physics,” *Phys. Rev. X* **9**, 041015 (2019).

<sup>4</sup> Yuto Ashida, Zongping Gong, and Masahito Ueda, “Non-hermitian physics,” *Advances in Physics* **69**, 249–435 (2020).

<sup>5</sup> Emil J. Bergholtz, Jan Carl Budich, and Flore K. Kunst, “Exceptional topology of non-hermitian systems,” *Rev. Mod. Phys.* **93**, 015005 (2021).

<sup>6</sup> Kazuki Yokomizo and Shuichi Murakami, “Non-bloch band theory of non-hermitian systems,” *Phys. Rev. Lett.* **123**, 066404 (2019).

<sup>7</sup> Kenta Esaki, Masatoshi Sato, Kazuki Hasebe, and Mahito Kohmoto, “Edge states and topological phases in non-hermitian systems,” *Phys. Rev. B* **84**, 205128 (2011).

<sup>8</sup> Yi Chen Hu and Taylor L. Hughes, “Absence of topological

insulator phases in non-hermitian  $pt$ -symmetric hamiltonians,” *Phys. Rev. B* **84**, 153101 (2011).

<sup>9</sup> V. M. Martinez Alvarez, J. E. Barrios Vargas, and L. E. F. Foa Torres, “Non-hermitian robust edge states in one dimension: Anomalous localization and eigenspace condensation at exceptional points,” *Phys. Rev. B* **97**, 121401 (2018).

<sup>10</sup> W D Heiss, “The physics of exceptional points,” *Journal of Physics A: Mathematical and Theoretical* **45**, 444016 (2012).

<sup>11</sup> Markus Müller and Ingrid Rotter, “Exceptional points in open quantum systems,” *Journal of Physics A: Mathematical and Theoretical* **41**, 244018 (2008).

<sup>12</sup> Huitao Shen, Bo Zhen, and Liang Fu, “Topological band theory for non-hermitian hamiltonians,” *Phys. Rev. Lett.* **120**, 146402 (2018).

<sup>13</sup> Mohammad-Ali Miri and Andrea Alù, “Exceptional points in optics and photonics,” *Science* **363**, eaar7709 (2019).

<sup>14</sup> Wei Wang, Xulong Wang, and Guancong Ma, “Non-hermitian morphing of topological modes,” *Nature* **608**, 50–55 (2022).

<sup>15</sup> Jan Carl Budich, Johan Carlström, Flore K. Kunst, and Emil J. Bergholtz, “Symmetry-protected nodal phases in non-hermitian systems,” *Phys. Rev. B* **99**, 041406 (2019).

<sup>16</sup> Ryo Okugawa and Takehito Yokoyama, “Topological exceptional surfaces in non-hermitian systems with parity-time and parity-particle-hole symmetries,” *Phys. Rev. B*



- 99**, 041202 (2019).
- 17 Tsuneya Yoshida, Robert Peters, Norio Kawakami, and Yasuhiro Hatsugai, “Symmetry-protected exceptional rings in two-dimensional correlated systems with chiral symmetry,” *Phys. Rev. B* **99**, 121101 (2019).
  - 18 M. Michael Denner, Anastasiia Skurativska, Frank Schindler, Mark H. Fischer, Ronny Thomale, Tomáš Bzdušek, and Titus Neupert, “Exceptional topological insulators,” *Nature Communications* **12**, 5681 (2021).
  - 19 Charles C. Wojcik, Xiao-Qi Sun, Tomáš Bzdušek, and Shanhui Fan, “Homotopy characterization of non-hermitian hamiltonians,” *Phys. Rev. B* **101**, 205417 (2020).
  - 20 Zhesen Yang, A. P. Schnyder, Jiangping Hu, and Ching-Kai Chiu, “Fermion doubling theorems in two-dimensional non-hermitian systems for fermi points and exceptional points,” *Phys. Rev. Lett.* **126**, 086401 (2021).
  - 21 Naomichi Hatano and David R. Nelson, “Localization transitions in non-hermitian quantum mechanics,” *Phys. Rev. Lett.* **77**, 570–573 (1996).
  - 22 Shunyu Yao and Zhong Wang, “Edge states and topological invariants of non-hermitian systems,” *Phys. Rev. Lett.* **121**, 086803 (2018).
  - 23 Motohiko Ezawa, “Non-hermitian boundary and interface states in nonreciprocal higher-order topological metals and electrical circuits,” *Phys. Rev. B* **99**, 121411 (2019).
  - 24 Ching Hua Lee and Ronny Thomale, “Anatomy of skin modes and topology in non-hermitian systems,” *Phys. Rev. B* **99**, 201103 (2019).
  - 25 Xi-Wang Luo and Chuanwei Zhang, “Higher-order topological corner states induced by gain and loss,” *Phys. Rev. Lett.* **123**, 073601 (2019).
  - 26 Dan S. Borgnia, Alex Jura Kruchkov, and Robert-Jan Slager, “Non-hermitian boundary modes and topology,” *Phys. Rev. Lett.* **124**, 056802 (2020).
  - 27 Kohei Kawabata, Masatoshi Sato, and Ken Shiozaki, “Higher-order non-hermitian skin effect,” *Phys. Rev. B* **102**, 205118 (2020).
  - 28 Kohei Kawabata, Nobuyuki Okuma, and Masatoshi Sato, “Non-bloch band theory of non-hermitian hamiltonians in the symplectic class,” *Phys. Rev. B* **101**, 195147 (2020).
  - 29 Stefano Longhi, “Unraveling the non-hermitian skin effect in dissipative systems,” *Phys. Rev. B* **102**, 201103 (2020).
  - 30 Kai Zhang, Zhesen Yang, and Chen Fang, “Correspondence between winding numbers and skin modes in non-hermitian systems,” *Phys. Rev. Lett.* **125**, 126402 (2020).
  - 31 Kai Zhang, Zhesen Yang, and Chen Fang, “Universal non-hermitian skin effect in two and higher dimensions,” *Nature Communications* **13**, 2496 (2022).
  - 32 Nobuyuki Okuma and Masatoshi Sato, “Non-hermitian topological phenomena: A review,” *Annual Review of Condensed Matter Physics* **14**, 83–107 (2023).
  - 33 Daichi Nakamura, Kazuya Inaka, Nobuyuki Okuma, and Masatoshi Sato, “Universal platform of point-gap topological phases from topological materials,” *Phys. Rev. Lett.* **131**, 256602 (2023).
  - 34 Ming-Hui Lu Xiujuan Zhang, Tian Zhang and Yan-Feng Chen, “A review on non-hermitian skin effect,” *Advances in Physics: X* **7**, 2109431 (2022).
  - 35 Kazuki Sone, Yuto Ashida, and Takahiro Sagawa, “Exceptional non-hermitian topological edge mode and its application to active matter,” *Nature Communications* **11**, 5745 (2020).
  - 36 Rijia Lin, Tommy Tai, Linhu Li, and Ching Hua Lee, “Topological non-hermitian skin effect,” *Frontiers of Physics* **18**, 53605 (2023).
  - 37 Flore K. Kunst, Elisabet Edvardsson, Jan Carl Budich, and Emil J. Bergholtz, “Biorthogonal bulk-boundary correspondence in non-hermitian systems,” *Phys. Rev. Lett.* **121**, 026808 (2018).
  - 38 Nobuyuki Okuma, Kohei Kawabata, Ken Shiozaki, and Masatoshi Sato, “Topological origin of non-hermitian skin effects,” *Phys. Rev. Lett.* **124**, 086801 (2020).
  - 39 Tony E. Lee, “Anomalous edge state in a non-hermitian lattice,” *Phys. Rev. Lett.* **116**, 133903 (2016).
  - 40 Simon Lieu, “Topological phases in the non-hermitian suschrieffer-heeger model,” *Phys. Rev. B* **97**, 045106 (2018).
  - 41 Jan Wiersig, “Response strengths of open systems at exceptional points,” *Phys. Rev. Res.* **4**, 023121 (2022).
  - 42 Fabrizio Minganti, Adam Miranowicz, Ravindra W. Chhajlany, and Franco Nori, “Quantum exceptional points of non-hermitian hamiltonians and liouvillians: The effects of quantum jumps,” *Phys. Rev. A* **100**, 062131 (2019).
  - 43 Fei Song, Shunyu Yao, and Zhong Wang, “Non-hermitian skin effect and chiral damping in open quantum systems,” *Phys. Rev. Lett.* **123**, 170401 (2019).
  - 44 Taiki Haga, Masaya Nakagawa, Ryusuke Hamazaki, and Masahito Ueda, “Liouvillian skin effect: Slowing down of relaxation processes without gap closing,” *Phys. Rev. Lett.* **127**, 070402 (2021).
  - 45 Kun Ding, Z. Q. Zhang, and C. T. Chan, “Coalescence of exceptional points and phase diagrams for one-dimensional  $\mathcal{PT}$ -symmetric photonic crystals,” *Phys. Rev. B* **92**, 235310 (2015).
  - 46 Tomoki Ozawa, Hannah M. Price, Alberto Amo, Nathan Goldman, Mohammad Hafezi, Ling Lu, Mikael C. Rechtsman, David Schuster, Jonathan Simon, Oded Zilberberg, and Iacopo Carusotto, “Topological photonics,” *Rev. Mod. Phys.* **91**, 015006 (2019).
  - 47 Christian E. Rüter, Konstantinos G. Makris, Ramy El-Ganainy, Demetrios N. Christodoulides, Mordechai Segev, and Detlef Kip, “Observation of parity–time symmetry in optics,” *Nature Physics* **6**, 192–195 (2010).
  - 48 Alois Regensburger, Christoph Bersch, Mohammad-Ali Miri, Georgy Onishchukov, Demetrios N. Christodoulides, and Ulf Peschel, “Parity–time synthetic photonic lattices,” *Nature* **488**, 167–171 (2012).
  - 49 Bo Zhen, Chia Wei Hsu, Yuichi Igarashi, Ling Lu, Ido Kaminer, Adi Pick, Song-Liang Chua, John D. Joannopoulos, and Marin Soljačić, “Spawning rings of exceptional points out of dirac cones,” *Nature* **525**, 354–358 (2015).
  - 50 Hengyun Zhou, Chao Peng, Yoseob Yoon, Chia Wei Hsu, Keith A. Nelson, Liang Fu, John D. Joannopoulos, Marin Soljačić, and Bo Zhen, “Observation of bulk fermi arc and polarization half charge from paired exceptional points,”

- Science **359**, 1009–1012 (2018).
- <sup>51</sup> Zin Lin, Adi Pick, Marko Lončar, and Alejandro W. Rodriguez, “Enhanced spontaneous emission at third-order dirac exceptional points in inverse-designed photonic crystals,” *Phys. Rev. Lett.* **117**, 107402 (2016).
- <sup>52</sup> Midya Parto, Yuzhou G. N. Liu, Babak Bahari, Mercedeh Khajavikhan, and Demetrios N. Christodoulides, “Non-hermitian and topological photonics: optics at an exceptional point,” *Nanophotonics* **10**, 403–423 (2021).
- <sup>53</sup> Ş. K. Özdemir, S. Rotter, F. Nori, and L. Yang, “Parity-time symmetry and exceptional points in photonics,” *Nature Materials* **18**, 783–798 (2019).
- <sup>54</sup> Janet Zhong, Kai Wang, Yubin Park, Viktor Asadchy, Charles C. Wojcik, Avik Dutt, and Shanhui Fan, “Non-trivial point-gap topology and non-hermitian skin effect in photonic crystals,” *Phys. Rev. B* **104**, 125416 (2021).
- <sup>55</sup> Xueyi Zhu, Huaiqiang Wang, Samit Kumar Gupta, Haijun Zhang, Biye Xie, Minghui Lu, and Yanfeng Chen, “Photonic non-hermitian skin effect and non-bloch bulk-boundary correspondence,” *Phys. Rev. Res.* **2**, 013280 (2020).
- <sup>56</sup> Weiwei Zhu and Jiangbin Gong, “Photonic corner skin modes in non-hermitian photonic crystals,” *Phys. Rev. B* **108**, 035406 (2023).
- <sup>57</sup> Bin Liu, Yang Li, Bin Yang, Xiaopeng Shen, Yuting Yang, Zhi Hong Hang, and Motohiko Ezawa, “Experimental observation of non-hermitian higher-order skin interface states in topological electric circuits,” *Phys. Rev. Res.* **5**, 043034 (2023).
- <sup>58</sup> Shuo Liu, Ruiwen Shao, Shaojie Ma, Lei Zhang, Oubo You, Haotian Wu, Yuan Jiang Xiang, Tie Jun Cui, and Shuang Zhang, “Non-hermitian skin effect in a non-hermitian electrical circuit,” *Research* **2021** (2021), 10.34133/2021/5608038.
- <sup>59</sup> T. Helbig, T. Hofmann, S. Imhof, M. Abdelghany, T. Kiessling, L. W. Molenkamp, C. H. Lee, A. Szameit, M. Greiter, and R. Thomale, “Generalized bulk–boundary correspondence in non-hermitian topoelectrical circuits,” *Nature Physics* **16**, 747–750 (2020).
- <sup>60</sup> Tobias Hofmann, Tobias Helbig, Frank Schindler, Nora Salgo, Marta Brzezińska, Martin Greiter, Tobias Kiessling, David Wolf, Achim Vollhardt, Anton Kabašič, Ching Hua Lee, Ante Bilušić, Ronny Thomale, and Titus Neupert, “Reciprocal skin effect and its realization in a topoelectrical circuit,” *Phys. Rev. Res.* **2**, 023265 (2020).
- <sup>61</sup> Tsuneya Yoshida, Tomonari Mizoguchi, and Yasuhiro Hatsugai, “Mirror skin effect and its electric circuit simulation,” *Phys. Rev. Res.* **2**, 022062 (2020).
- <sup>62</sup> Nobuyuki Okuma and Masatoshi Sato, “Non-hermitian skin effects in hermitian correlated or disordered systems: Quantities sensitive or insensitive to boundary effects and pseudo-quantum-number,” *Phys. Rev. Lett.* **126**, 176601 (2021).
- <sup>63</sup> Tsuneya Yoshida, “Real-space dynamical mean field theory study of non-hermitian skin effect for correlated systems: Analysis based on pseudospectrum,” *Phys. Rev. B* **103**, 125145 (2021).
- <sup>64</sup> Tsuneya Yoshida, Robert Peters, and Norio Kawakami, “Non-hermitian perspective of the band structure in heavy-fermion systems,” *Phys. Rev. B* **98**, 035141 (2018).
- <sup>65</sup> Tsuneya Yoshida, Robert Peters, Norio Kawakami, and Yasuhiro Hatsugai, “Exceptional band touching for strongly correlated systems in equilibrium,” *Progress of Theoretical and Experimental Physics* **2020**, 12A109 (2020).
- <sup>66</sup> Yoshihiro Michishita, Tsuneya Yoshida, and Robert Peters, “Relationship between exceptional points and the kondo effect in  $f$ -electron materials,” *Phys. Rev. B* **101**, 085122 (2020).
- <sup>67</sup> Yoshihiro Michishita and Robert Peters, “Equivalence of effective non-hermitian hamiltonians in the context of open quantum systems and strongly correlated electron systems,” *Phys. Rev. Lett.* **124**, 196401 (2020).
- <sup>68</sup> Shin Kaneshiro, Tsuneya Yoshida, and Robert Peters, “ $Z_2$  non-hermitian skin effect in equilibrium heavy-fermion systems,” *Phys. Rev. B* **107**, 195149 (2023).
- <sup>69</sup> Yuki Nagai, Yang Qi, Hiroki Isobe, Vladyslav Kozii, and Liang Fu, “Dmft reveals the non-hermitian topology and fermi arcs in heavy-fermion systems,” *Phys. Rev. Lett.* **125**, 227204 (2020).
- <sup>70</sup> Roman Rausch, Robert Peters, and Tsuneya Yoshida, “Exceptional points in the one-dimensional hubbard model,” *New Journal of Physics* **23**, 013011 (2021).
- <sup>71</sup> L. Crippa, J. C. Budich, and G. Sangiovanni, “Fourth-order exceptional points in correlated quantum many-body systems,” *Phys. Rev. B* **104**, L121109 (2021).
- <sup>72</sup> Vladyslav Kozii and Liang Fu, “Non-hermitian topological theory of finite-lifetime quasiparticles: Prediction of bulk fermi arc due to exceptional point,” (2017), arXiv:1708.05841 [cond-mat.mes-hall].
- <sup>73</sup> A. A. Zyuzin and A. Yu. Zyuzin, “Flat band in disorder-driven non-hermitian weyl semimetals,” *Phys. Rev. B* **97**, 041203 (2018).
- <sup>74</sup> Huitao Shen and Liang Fu, “Quantum oscillation from in-gap states and a non-hermitian landau level problem,” *Phys. Rev. Lett.* **121**, 026403 (2018).
- <sup>75</sup> Robert Peters, Kazuhiro Kimura, Yoshihiro Michishita, Tsuneya Yoshida, and Norio Kawakami, “Surface exceptional points in a topological kondo insulator,” *Phys. Rev. B* **104**, 235153 (2021).
- <sup>76</sup> Frank Schindler, Ashley M. Cook, Maia G. Vergniory, Zhi-jun Wang, Stuart S. P. Parkin, B. Andrei Bernevig, and Titus Neupert, “Higher-order topological insulators,” *Science Advances* **4**, eaat0346 (2018).
- <sup>77</sup> Biye Xie, Hai-Xiao Wang, Xiujuan Zhang, Peng Zhan, Jian-Hua Jiang, Minghui Lu, and Yanfeng Chen, “Higher-order band topology,” *Nature Reviews Physics* **3**, 520–532 (2021).
- <sup>78</sup> Ryo Okugawa, Ryo Takahashi, and Kazuki Yokomizo, “Second-order topological non-hermitian skin effects,” *Phys. Rev. B* **102**, 241202 (2020).
- <sup>79</sup> Elisabet Edvardsson, Flore K. Kunst, and Emil J. Bergholtz, “Non-hermitian extensions of higher-order topological phases and their biorthogonal bulk-boundary correspondence,” *Phys. Rev. B* **99**, 081302 (2019).
- <sup>80</sup> Tao Liu, Yu-Ran Zhang, Qing Ai, Zongping Gong, Ko-

- hei Kawabata, Masahito Ueda, and Franco Nori, “Second-order topological phases in non-hermitian systems,” *Phys. Rev. Lett.* **122**, 076801 (2019).
- <sup>81</sup> Naomichi Hatano and David R. Nelson, “Vortex pinning and non-hermitian quantum mechanics,” *Phys. Rev. B* **56**, 8651–8673 (1997).
- <sup>82</sup> Robert Peters, Tsuneya Yoshida, and Norio Kawakami, “Magnetic states in a three-dimensional topological kondo insulator,” *Phys. Rev. B* **98**, 075104 (2018).
- <sup>83</sup> Walter Metzner and Dieter Vollhardt, “Correlated lattice fermions in  $d = \infty$  dimensions,” *Phys. Rev. Lett.* **62**, 324–327 (1989).
- <sup>84</sup> E. Müller-Hartmann, “Correlated fermions on a lattice in high dimensions,” *Zeitschrift für Physik B Condensed Matter* **74**, 507–512 (1989).
- <sup>85</sup> Antoine Georges, Gabriel Kotliar, Werner Krauth, and Marcelo J. Rozenberg, “Dynamical mean-field theory of strongly correlated fermion systems and the limit of infinite dimensions,” *Rev. Mod. Phys.* **68**, 13–125 (1996).
- <sup>86</sup> Robert Peters, Tsuneya Yoshida, Hirofumi Sakakibara, and Norio Kawakami, “Coexistence of light and heavy surface states in a topological multiband kondo insulator,” *Phys. Rev. B* **93**, 235159 (2016).
- <sup>87</sup> Ralf Bulla, Theo A. Costi, and Thomas Pruschke, “Numerical renormalization group method for quantum impurity systems,” *Rev. Mod. Phys.* **80**, 395–450 (2008).
- <sup>88</sup> Robert Peters, Thomas Pruschke, and Frithjof B. Anders, “Numerical renormalization group approach to green’s functions for quantum impurity models,” *Phys. Rev. B* **74**, 245114 (2006).